Journal of Catalysis 266 (2009) 92–97

Contents lists available at ScienceDirect

Journal of Catalysis

journal homepage: www.elsevier.com/locate/jcat

A highly dispersed Pd–Mg/SiO_2 catalyst active for methanation of CO_2

Jung-Nam Park [a,b], Eric W. McFarland [a,*]

[a] Department of Chemical Engineering, University of California, Santa Barbara, CA 93106-5080, USA
[b] Department of Chemistry, Sungkyunkwan University, Suwon 440-746, South Korea

ARTICLE INFO

Article history:
Received 10 February 2009
Revised 15 May 2009
Accepted 22 May 2009
Available online 13 June 2009

Keywords:
CO_2 activation
Methanation
Pd
Mg
Reverse microemulsion

ABSTRACT

A catalyst formed as an aggregate of highly dispersed palladium and magnesium in silica was prepared using a reverse microemulsion synthesis. After calcination, the catalyst consists predominately of Pd containing particles 5 to 10 nm in size distributed within an amorphous oxide of Mg and Si. The catalytic activity and selectivity of the Pd–Mg/SiO_2 catalyst for CO_2 methanation were characterized and compared to several other catalyst preparations. At 450 °C, the Pd–Mg/SiO_2 catalyst had greater than 95% selectivity to CH_4 at a carbon dioxide conversion of 59%, while similar catalysts without Mg have activity only for CO_2 reduction to CO, and the Mg- and Si-containing oxide (without a transition metal) are relatively inactive. The results support a synergistic effect between the Pd and the Mg/Si oxide.

Published by Elsevier Inc.

1. Introduction

The potential utilization of CO_2 as an abundant and inexpensive chemical feedstock is of widespread interest [1]. Carbon dioxide has been used as an oxidant for the dehydrogenation of ethylbenzene to styrene [2], and in a familiar Sabatier reaction for the hydrogenation of CO_2,

$$CO_2(g) + 4H_2(g) \rightarrow CH_4(g) + 2H_2O(g), \quad \Delta G_{0\,298K} = -27 \text{ kcal mol}^{-1}.$$

The methanation of CO_2 has a range of applications including the production of synthetic natural gas [3] and the removal of trace amounts of CO_2 in hydrogen feeds for ammonia synthesis. There have been proposed applications for space travel to obtain drinking water by combining the on-board hydrogen rocket fuel with carbon dioxide produced by the astronauts. In all applications, increasing the rate and selectivity of the reduction pathway is highly desirable.

The methanation reaction is exothermic; however, an 8-electron process is required to reduce the fully oxidized carbon to methane and there are significant kinetic limitations which require a catalyst to achieve acceptable rates and selectivities. Extensive studies have been conducted on several metal-based catalytic systems using Ni [4–7], Ru [8–11], and Rh [12] as well as metal oxides [13,14].

A unique activity has been observed using bimetallic and bifunctional catalyst concepts. A Ni(II)-Ferrite catalyst with a spinel structure has been shown to be active for CO_2 methanation with a high selectivity at 300 °C [15]; however, the ultra-fine particulate catalysts were unstable and rapidly sintered. Sehested et al. have demonstrated that a Ni–Fe alloy catalyst is more selective for the conversion of CO_2 to CH_4 than a pure nickel catalyst at 330 °C in excess hydrogen [16]. de Leitenburg et al. have investigated why Ru or Rh supported on CeO_2 produces only CH_4 as the reaction product whereas Pt, Pd, and Ir give both CO and CH_4 over a range of temperatures up to 630 °C showing the maximum yield of CH_4 at approximately 450 °C [14]. A bifunctional mechanism has been invoked to explain the behavior of iron- and ceria-containing catalysts [17,18]. The hydrogen is thought to react with oxygen in the metal oxide to produce water and reduce the metal species leaving behind oxygen vacancies which are the sites for CO_2 reduction.

For efficient utilization of bifunctional pathways intimate mixing of the heterospecies is required and phase separation is minimized. Recently, reverse microemulsion methods have been utilized to achieve highly dispersed catalysts [19,20]. In a reverse microemulsion synthesis, the reverse micelles form nanometer-size droplets with an aqueous phase core in which the catalyst precursor is soluble. The droplets are dispersed in a continuous oil phase. By the addition of precursors from several species, the aggregate solids formed within the micelles can be used to directly contact multiple species and form uniformly dispersed bimetallic or mixed oxide nanoparticles [21,22]. He et al. prepared CeO_2/ZnO mixed oxide catalysts using reverse microemulsions for an oxidative coupling of CH_4 with CO_2 which showed significantly higher activity than CeO_2/ZnO catalysts prepared by conventional impregnation methods [22]. Other catalysts synthesized using reverse microemulsions have shown improved activities compared

* Corresponding author.
E-mail address: mcfar@engineering.ucsb.edu (E.W. McFarland).

0021-9517/$ - see front matter Published by Elsevier Inc.
doi:10.1016/j.jcat.2009.05.018

to those synthesized by conventional impregnation methods for applications in hydrogenation [23] and oxidation [24].

We are investigating Pd–Mg/SiO_2 as a bifunctional catalyst for CO_2 methanation motivated by the properties of Pd to dissociate molecular hydrogen [25,26] and make available hydrogen atoms for the subsequent transfer and reaction with activated surface carbonate species formed by the reaction of CO_2 on a Mg-containing oxide [27–29]. The conceptual approach is to provide an alternative pathway to potentially minimize the CO byproduct by using metal oxides that inhibit CO desorption. To create intermixed Pd and Mg sites, the reverse microemulsion synthesis route is used. In this report, we address the following questions: (1) Is a highly dispersed and intermixed Pd–Mg/SiO_2 catalyst active for CO_2 methanation? (2) What is the sensitivity of the catalyst performance to the synthesis method? (3) How does the activity and selectivity compare to the individual Pd and Mg oxide components and other methanation catalysts?

2. Experimental

2.1. Catalyst synthesis

The Pd–Mg/SiO_2 catalyst was synthesized from a reverse microemulsion (ME) by adding a mixture of $Pd(NO_3)_2{\cdot}H_2O$ (Aldrich, 7 ml, 0.028 M) and a $Mg(NO_3)_2{\cdot}H_2O$ (Aldrich, 3 mL, 0.169 M) to a vigorously stirred solution containing a non-ionic surfactant (40 mL, Igepal CO-520, Aldrich) and cyclohexane (100 mL, Fisher Scientific). While stirring, Hydrazine (64 μL, Aldrich 98%) was added and the mixture was stirred for another hour. A NH_4OH solution (EMD 28%) was then added to adjust the pH to 11. After another hour of stirring a mixture of TEOS (tetraethyl orthosilicate, 0.995 mL, Acros organic) and C_{18} TMS (n-octadecyl trimethoxysilane, 0.357 mL, Gelest Inc.) was added dropwise. Hydrolysis and condensation of the silica precursors were allowed to proceed in the stirred mixture for 3 days at 20 °C. After condensation, the Pd–Mg/SiO_2 was precipitated and washed with ethanol. The ethanol wash followed by centrifugation was repeated thrice. The Pd–Mg/SiO_2 was dried at 100 °C and was calcined at 550 °C in air for 6 h; the heating rate was 1 °C min^{-1}. The Pd/SiO_2 (ME) [30], Mg/SiO_2, and Ni/SiO_2 catalysts were synthesized using nitrate precursors; $Pd(NO_3)_2{\cdot}H_2O$ (Aldrich, 10 mL, 0.02 M), $Mg(NO_3)_2{\cdot}H_2O$ (Aldrich, 10 mL, 0.02 M), and a $Ni(NO_3)_2{\cdot}H_2O$ (Aldrich, 10 mL, 0.02 M), respectively. For the Pd–Ni/SiO_2, Pd–Fe/SiO_2, and Pd–Li/SiO_2 catalysts synthesis was from mixed solutions of the $Pd(NO_3)_2{\cdot}H_2O$ (Aldrich, 7 mL, 0.028 M) with $Ni(NO_3)_2{\cdot}H_2O$ (Aldrich), $Fe(NO_3)_2{\cdot}H_2O$ (Aldrich), or $Li(NO_3)_2{\cdot}H_2O$ (Aldrich, 3 mL, 0.169 M), respectively. The silica impregnated with Pd catalyst, Pd/SiO_2 (IMP), was synthesized on silica spheres produced from a reverse microemulsion (ME) identical to that described above for the Pd/SiO_2 (ME), with the Pd precursor replaced with NH_4OH solution and without a reducing agent [30]. SiO_2 spheres (0.35 g) were added to a solution of $Pd(NO_3)_2{\cdot}H_2O$ (0.05 g) in 40 ml of water and were stirred for 4 h at 80 °C then dried at 110 °C and calcined at 550 °C in air for 6 h; the heating rate was 1 °C min^{-1}. The Pd loading was 6.2 wt% and the loading of the second metal was 3.6 wt%.

2.2. Catalyst characterization

The catalyst morphology was investigated using transmission electron microscopy, TEM (JEN2100F, JEOL) and the elemental distribution was monitored with energy dispersive X-ray spectroscopy, EDS, with a system integrated to the TEM (Oxford INCA). To determine the particle size distribution and average particle size, 100 particles were measured from the TEM images. Errors were taken as the standard deviation of the particle sizes. X-ray diffraction, XRD, was performed on selected samples over the scattering range of $30 \leqslant 2\theta \leqslant 75$ with steps of 0.017° using Cu Kα radiation (Philips X'Pert Pro X-ray diffractometer). The surface area was estimated using BET analysis of the N_2 adsorption isotherms (Micromeritics, Model ASAP 2400).

2.3. Catalytic activity

Methanation of CO_2 was performed with 0.1 g of catalyst (40 to 60 mesh) in a 6 mm diameter fixed bed reactor. The reactions were performed at atmospheric pressure over a temperature range of 25 to 450 °C using a mixture of carbon dioxide and hydrogen at a ratio of CO_2: H_2 = 1:4 (flow rate = 10.2 cm^3 min^{-1}) mixed with 2 cm^3 min^{-1} Ar. The space time was 1.1 s. The catalyst samples were pretreated at 450 °C in H_2 prior to reaction. The product gas stream was analyzed by parallel gas chromatography (GC, SRI, Inc.) with a 5 Å molecular sieve column, and mass spectrometry (SRS, Inc.). To determine conversion and selectivity, the products were collected after one hour of steady-state operation at each temperature. The conversions of carbon dioxide and hydrogen were determined from the ratios of the difference in the molar flow rates in the feed minus the product to the feed molar flow rate. The molar flow rates were assumed proportional to their concentration in the gas streams. Selectivities were calculated as moles of individual products produced per mole of total products (methane plus carbon monoxide) produced. The yields were determined as the product of the conversion and the selectivity. For temperature-programed methanation, the heating rate was 7.5 °C min^{-1}.

3. Results and discussion

3.1. Catalyst characterization

The catalyst loadings and BET surface areas are listed out in Table 1. The surface areas of the Pd/SiO_2 and Pd(Imp)/SiO_2 were found to be 185 and 134 m^2/g, respectively. The surface areas of catalysts synthesized from reverse microemulsions were in the range 110 to 190 m^2 g^{-1}.

The morphology of the Pd–Mg/SiO_2 catalysts characterized by TEM is shown in Fig. 1. The micrographs show that the as-synthesized Pd–Mg/SiO_2 catalyst after calcination at 550 °C in air for 6 h contains well-dispersed electron-dense particles identified as containing Pd by EDS within a matrix of less dense solid that does not appear crystalline, Fig. 1a. The particles appear uniform in shape with a diameter of approximately 5.5 ± 2.0 nm. Features within the image are consistent with the remnants of silica shells surrounding the electron-dense centers, however, aggregation has occurred. After reaction with CO_2 and hydrogen for 10 h, the particles remain well dispersed and though the presence of larger particles is observed, a large fraction of the Pd-containing nanoparticles

Table 1
Catalyst loadings and BET surface areas.

Catalyst	Pd (wt%)	Second metal (wt%)	BET surface area (m^2 g^{-1})
Pd/SiO_2	Pd: 6.2	–	185
Pd(Imp)/SiO_2[a]	Pd: 6.2	–	134
Mg/SiO_2	Mg: 6.2	–	123
Pd–Mg/SiO_2	Pd: 6.2	Mg: 3.6	189
Mg(Imp)/Pd/SiO_2[b]	Pd: 6.2	Mg: 3.6	80
Pd–Fe/SiO_2	Pd: 6.2	Fe: 3.6	188
Pd–Ni/SiO_2	Pd: 6.2	Ni: 3.6	155
Ni/SiO_2	Ni: 6.2	–	169
Pd–Li/SiO_2	Pd: 6.2	Li: 3.6	109

[a] Palladium was impregnated on SiO_2 spheres.
[b] Magnesium was impregnated on Pd/SiO_2 from a reverse microemulsion.

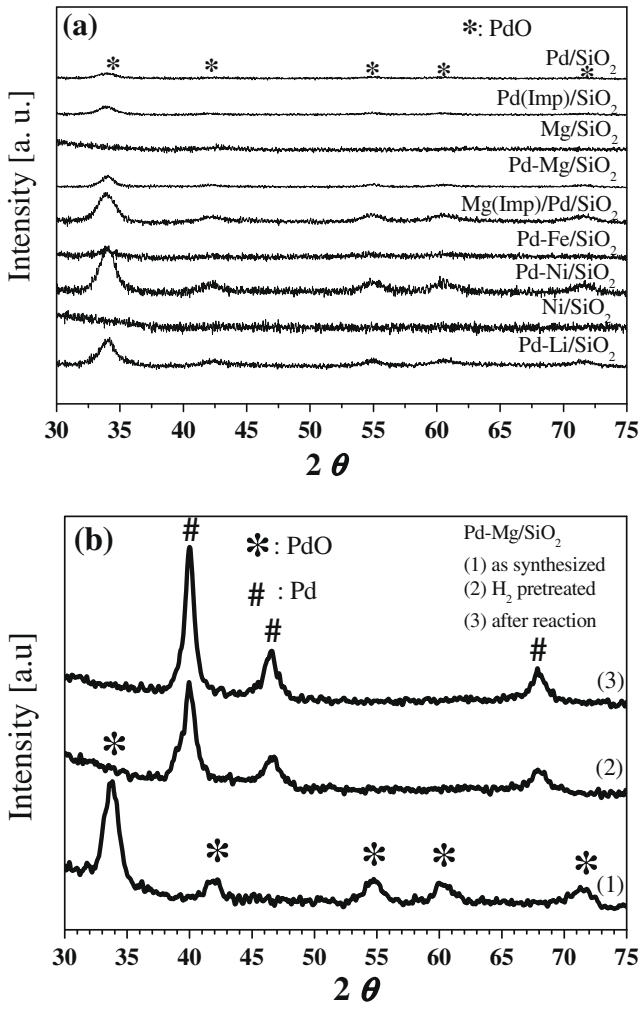

Fig. 1. (a) XRD data obtained from all the catalysts studied after initial synthesis and calcination, (b) XRD data obtained from the Pd–Mg/SiO_2 catalyst as synthesized (and calcined), following H_2 pretreated, and after reaction for approximately 10 h.

maintain a size of approximately 5.5 nm, Fig. 1b. We speculate that there is a relatively small population of Pd particles that were not fully encapsulated by the Mg/Si oxide that were able to sinter; however, there remains a significant population of Pd-containing nanoparticles that remain stable. EDS performed within localized ~20 nm regions of the image, Fig. 1c and d, indicate the presence of Pd, Mg, and Si. The TEM images are consistent with a stable well-dispersed aggregate of Pd-containing nanoparticles in an amorphous oxide matrix.

The XRD data for the as-synthesized catalysts after calcination at 550 °C in air for 6 h are shown in Fig. 2a. Broad reflections at approximately 25° (not shown) were consistent with an amorphous metal oxide phase or very small nanocrystallites. When present, reflections for the Pd phase were consistent with those for palladium oxide (PdO (101) at 33.9° 2θ and Pd (110) at 41.9° 2θ). We have previously shown the presence of the same PdO phase in as-synthesized Pd/SiO_2 and $Pd(Imp)/SiO_2$ catalysts [30]. The palladium phase in Pd–X/SiO_2 (X = Li, Mg, Fe, Ni) was also observed to be PdO and the absence of reflections for the second metal (X) phase is consistent with an amorphous or nanocrystalline phase. There was no evidence for a crystalline phase of Ni or Mg in the Ni/SiO_2 or Mg/SiO_2 catalysts calcined at 550 °C. An estimate of the size of the Pd particles was made using the Scherrer equation and found to be in reasonable agreement with the TEM's at approximately 7 to 10 nm. Fig. 2b shows the XRD data from the Pd–Mg/SiO_2 catalysts as synthesized, after H_2 pretreated, and after the methanation reaction. Not surprisingly, the PdO is reduced to Pd metal after H_2 pretreatment and after 10 h under methanation reaction conditions the metallic Pd phase remains (Pd (111) at 40.1° 2θ and (200) at 46.7° 2θ). XPS performed ex situ before and after reaction (data not shown) was consistent with a metallic Pd and oxide containing Mg and Si. The particle sizes of the Pd aggregates in Pd–Mg/SiO_2 after reaction for more than 10 hours as calculated by the Scherrer equation from the XRD data indicate that there is an increase in the Pd phase size from ~10 nm in the as-synthesized catalyst to ~19 nm after reaction. This may represent the superposition of the sharper reflections from the larger sintered particles on the broader reflection from the smaller, stable aggregates observed by TEM.

3.2. Catalyst activity

Table 2 shows the data for the conversions of CO_2 and H_2 and the selectivities and yields to CH_4 and CO over various catalysts at 450 °C. At 450 °C, Pd/SiO_2 is active for CO_2 reduction to CO in the presence of H_2 and Mg/SiO_2 (without Pd) is relatively inactive; however, the Pd–Mg/SiO_2 catalyst had greater than 95% selectivity to CH_4 at a carbon dioxide conversion of 59%. The CO_2 and H_2 conversion on the Pd–Mg/SiO_2 catalyst synthesized from the reverse microemulsion was significantly higher than that observed on the Pd/SiO_2, Mg/SiO_2, or the other catalysts. The compositionally identical $Mg/Pd/SiO_2$ catalyst synthesized by Mg impregnation of the Pd/SiO_2 catalyst (made by reverse microemulsion) was less active and less selective than when both Mg and Pd were introduced simultaneously in the reverse microemulsion. The Pd–Mg/SiO_2 catalyst synthesized from the reverse microemulsion has significantly greater contact between Pd-containing nanoparticles and Mg-containing oxide. The catalyst made from the reverse microemulsion also showed larger CO_2 conversion and methane selectivity compared to the same catalyst prepared by impregnation [19,20]. The Pd–Ni/SiO_2 catalyst showed higher conversion and selectivity to CH_4 compared to Ni/SiO_2. On the other hand, Pd–Fe/SiO_2 showed the highest selectivity to CO (97%) at high CO_2 conversion (45%). The overall conversion of CO_2 for the several catalysts followed the general ordering Pd–Mg/SiO_2 > Pd–Ni/SiO_2 > Pd–Fe/SiO_2 > Pd–Li/SiO_2 > Pd/SiO_2 > Ni/SiO_2 ≫ Mg/SiO_2, while the selectivity to CH_4 decreased in the following order Pd–Mg/SiO_2 > Pd–Ni/SiO_2 > Pd–Li/SiO_2 > $Mg(Imp)/Pd/SiO_2$ > Ni/SiO_2 > Pd–Li/SiO_2 > Pd/SiO_2 = Mg/SiO_2.

The data in Table 2 are consistent with the reaction stoichiometries and the requisite increase in H_2 conversion is coincident with an increase in selectivity for methane production. The reaction proposed by Choe et al. [31] in Scheme 1suggests that the alternative product, CO, is likely produced as an intermediate during methanation. The stability of the CO moiety on the catalyst will determine whether or not the CO will desorb or progress for further reduction. The CO dissociation is thought to be rate determining for the remaining reduction steps. It was observed that with the carbonate forming catalyst combinations, Pd–X/SiO_2 (X = Mg, Li) there was a high selectivity to CH_4 (95%, 88%) and a corresponding higher H_2 conversion (27%, 22%) as the intermediate carbonate XO_2–CO is stabilized and CO desorption is inhibited. The Pd–Fe/SiO_2 catalyst is active for CO_2 activation at high conversion; however, unlike the Pd–Mg/SiO_2 catalyst, there is no means for stabilizing the carbonate on the Fe/Si oxide. The hydrogen will react with the hematite surface oxygen to produce water and form oxygen vacancies which will activate additional CO_2 to fill the vacancy and produce CO. The pathway to further dissociate CO does not compete significantly with CO desorption. Utilization of H_2 is low

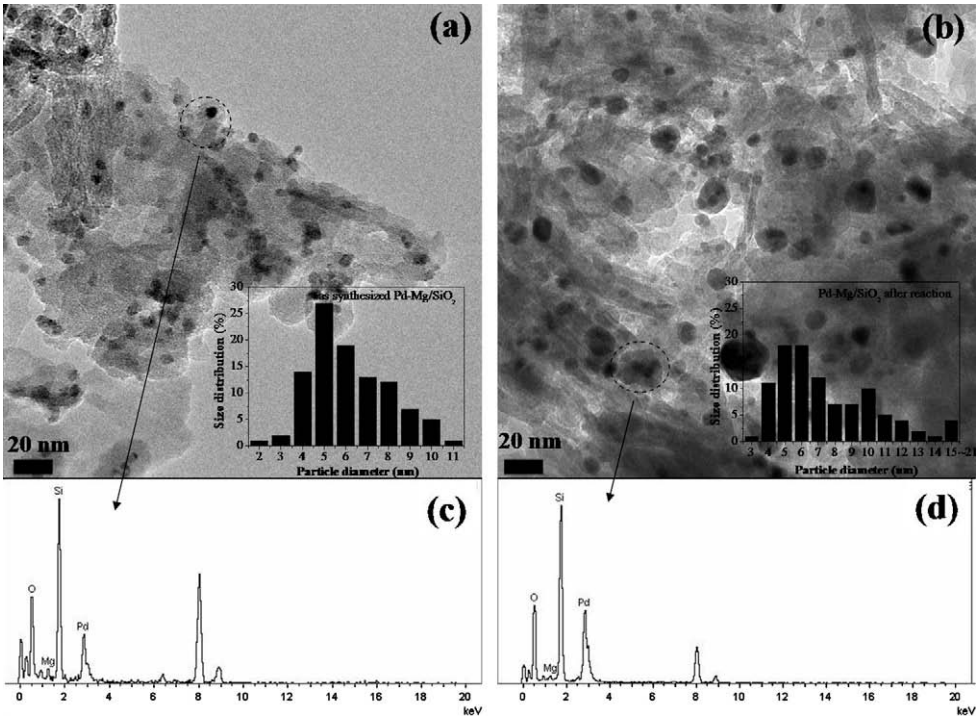

Fig. 2. Images obtained by TEM of the Pd–Mg/SiO_2 catalyst (a) before, and (b) after reaction with respective particle size distributions determined from 100 electron-dense particles. EDS results from the regions indicated in the TEM's are shown below with the elemental distributions, (c) and (d).

Table 2
Conversion, selectivity, and yield for the reaction of CO_2 and H_2 over 0.1 g of the studied catalysts at 450 °C.

Catalyst	CO_2 conversion (%)	H_2 conversion (%)	Selectivity (%)		Yield (%)	
			CH_4	CO	CH_4	CO
Pd/SiO_2	40.8	11.4	10.4	89.6	4.3	36.5
$Pd(Imp)/SiO_2$	40.6	9.6	6.5	93.5	2.6	38.0
Mg/SiO_2	0.8	6.7	10.3	89.7	0.1	0.7
$Pd–Mg/SiO_2$	59.2	26.9	95.3	4.7	56.4	2.8
$Mg(Imp)/Pd/SiO_2$	40.0	15.3	76.2	23.8	30.4	9.5
$Pd–Fe/SiO_2$	44.7	5.7	2.8	97.2	1.3	43.4
$Pd–Ni/SiO_2$	50.5	23.4	89.0	11.0	44.9	5.6
Ni/SiO_2	36.8	14.8	81.8	18.2	30.1	7.0
$Pd–Li/SiO_2$	42.6	21.8	88.5	11.5	37.7	4.9

Reaction conditions: space time = 1.1 s, mole ratio of reactants $H_2/CO_2 = 4$, flow rate = 10.2 $cm^3\ min^{-1}$. The standard error in conversion and selectivity was estimated as ±0.3% and 0.5%, respectively, from three repeat steady-state measurements at each temperature.

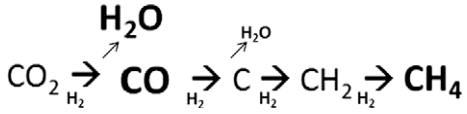

Scheme 1. A possible reaction pathway for CO_2 reduction to methane with hydrogen. A catalyst that facilitates the rate-limiting dissociation of CO without releasing CO to the gas phase is necessary for methane formation.

since the formation of CO requires only one H_2 while that of methanation requires four.

The activities of the individual components of the Pd–Mg/SiO_2 catalyst are also listed out in Table 2. The Pd/SiO_2 catalyst was reasonably active for CO_2 reduction to CO; however, an intermediate carbonate is not anticipated and minimal methane production was observed. Carbon dioxide will only weakly adsorb molecularly on silica, however; on Pd/SiO_2, CO_2 has been shown to undergo dissociative chemisorption [32] and in the presence of atomic hydrogen from dissociative chemisorptions of H_2 on Pd, the atomic oxygen from CO_2dissociation readily forms water. The CO remaining on the surface might undergo further reduction; however, the predominate pathway at 450 °C will be CO desorption. The oxidized Mg in the Mg/SiO_2 will react with CO_2 to form a carbonate which will be stable in the absence of atomic hydrogen.

Fig. 3 shows the CH_4 (a) and CO (b) partial pressures measured by mass spectroscopy during temperature-programed reaction of $CO_2 + 4\ H_2$ on the several catalysts studied. All catalysts produced CO by approximately 300 °C; however, a maximum CO production rate was observed at approximately 350 °C for Pd–Mg/SiO_2 and by 450 °C almost no CO was formed. Both Pd/SiO_2 and the less active Mg/SiO_2 catalysts produce primarily CO at all temperatures. The Pd–Fe/SiO_2 catalyst is highly active for CO_2 reduction to CO. The Ni-based catalyst is active with both CO and CH_4 production with increasing temperature; however, the Pd–Ni/SiO_2 catalyst is more active and selective for CH_4 than Ni/SiO_2.

In as much as higher temperature is required for methane formation, Fig. 3a, is consistent with the need to overcome the rate limiting CO dissociation barrier. Although our work has not specifically investigated the mechanism of the Pd–Mg/SiO_2 catalyst, we can draw on work from Yoshida et al. [33] who investigated the hydrogenation of calcium carbonate and showed that Pd or Ir catalysts provided H atom spillover to hydrogenate the carbonate at temperatures far below their uncatalyzed hydrogenation temperatures. In the Pd–Mg/SiO_2 catalyst, we speculate that Pd similarly provides atomic hydrogen to Mg carbonates to form methane and upon the desorption of the methane the carbonate is reformed by gas phase CO_2, Scheme 2.

Fig. 4a compares the conversion of CO_2 and H_2 over Pd–Mg/SiO_2 at several reaction temperatures. Raising the reaction temperature facilitates the CO dissociation step such that further hydrogenation can occur at a rate greater than CO desorption. The CO_2 and H_2 conversions increase from 9.8% and 3.2 % at 300 °C to 59.2% and 26.9%

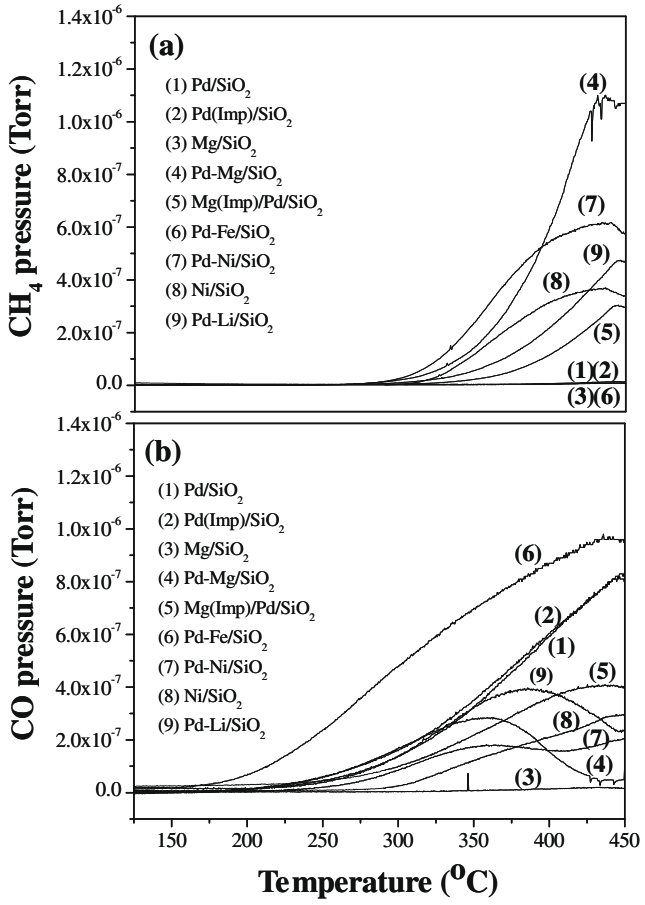

Fig. 3. Mass spectrometer measured partial pressures of products from reaction of hydrogen and carbon dioxide over 0.1 g of several catalysts. (a) CH_4 (mass number: 15), (b) CO (mass number: 28). Reaction conditions: space time = 1.1 s, mole ratio of reactants $H_2/CO_2 = 4$, flow rate = 10.2 $cm^3\ min^{-1}$.

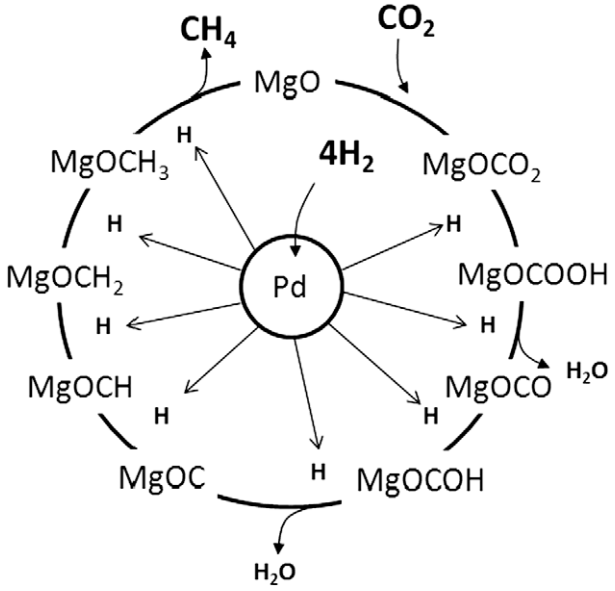

Scheme 2. A potential bifunctional mechanism for Pd–Mg/SiO_2 whereby spillover of atomic hydrogen from Pd in intimate contact with Mg carbonate sequentially hydrogenates carbon until the product methane desorbs.

at 450 °C, respectively, with the methanation channel activated; and CO selectivity and yield are decreased and CH_4 selectivity and yield are increased with increasing reaction temperature

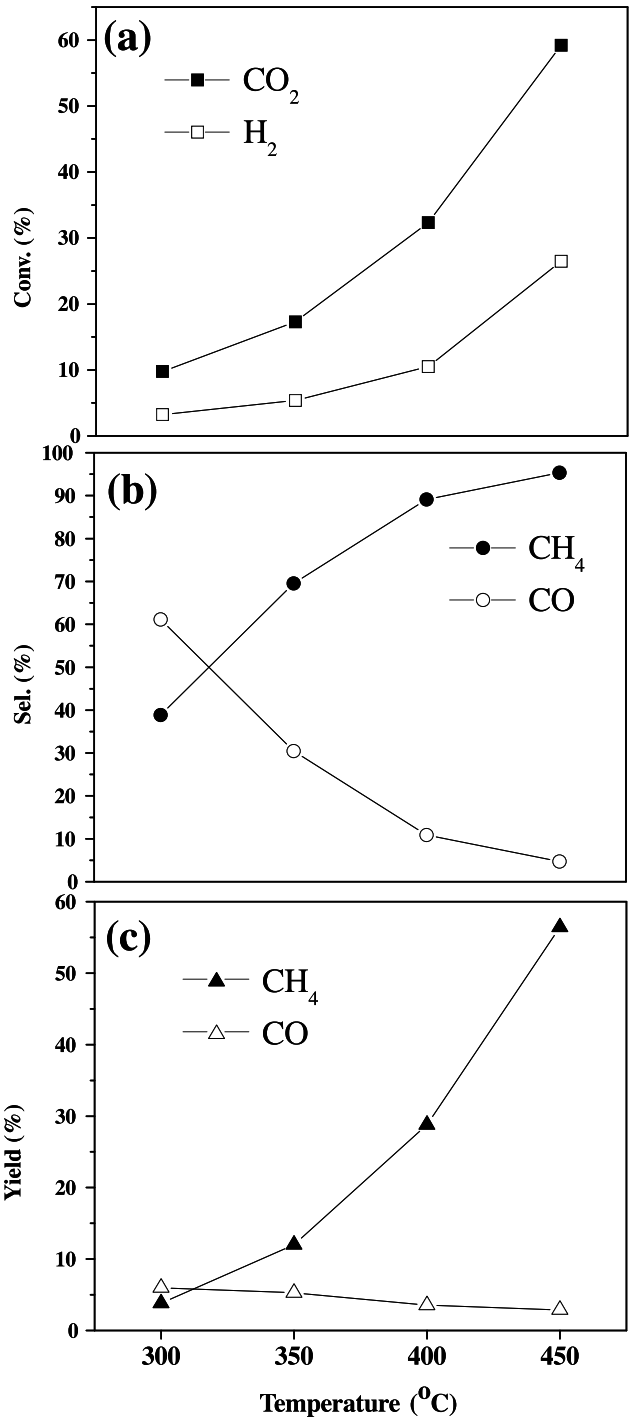

Fig. 4. Steady-state performance of Pd–Mg/SiO_2 catalysts measured over 1 h at different temperatures. (a) conversion, (b) selectivity, and (c) yield. Reaction conditions: catalyst weight = 0.1 g, space time = 1.1 s, mole ratio of reactants $H_2/CO_2 = 4$, flow rate = 10.2 $cm^3\ min^{-1}$.

(Fig. 4b and c). The CH_4 selectivity of 38.8% at 300 °C is increased to 95.3% at 450 °C, whereas CO selectivity of 61.1% at 300 °C is decreased to 4.7% at 450 °C. The CH_4 yield increased to 56.4% at 450 °C. The stability in performance was monitored for more than 9 h on stream and the conversion and selectivity show no significant degradation, Fig. S1, which is consistent with the observations by TEM, Fig. 2b.

An Arrhenius plot (Fig. S2) can help to clarify trends observed in the temperature-programed reaction data from Fig. 3 which

supports a low effective activation barrier for the low temperature partial reduction activity of the Pd–Fe/SiO_2 catalyst and the more favorable methanation pathway for the Pd–Mg/SiO_2 catalyst at the comparatively lower temperatures. From the temperature-programed reaction data the apparent activation energy (E_a) for the reaction of carbon dioxide with hydrogen on the Pd–Mg/SiO_2 catalyst is calculated from a least-squares fit of the logarithm of the carbon dioxide conversion versus $1/T$ as 82.0 ± 0.2 kJ mol^{-1} where the error was estimated as the standard deviation of the fit. This value was somewhat greater than the value reported for E_a over a Ru catalyst (74 kJ mol^{-1}) [11]. Although CO is formed at low temperatures on Pd–Mg/SiO_2 with a low apparent activation energy 52.7 ± 0.2 kJ/mol which is comparable to E_a calculated for the Pd–Fe/SiO_2 catalyst (50.8 ± 0.2 kJ/mol), the higher temperature allows the dissociation of the CO to occur for methanation with an E_a calculated from the methane production rate on Pd–Mg/SiO_2 as 106.9 ± 0.5 kJ/mol.

4. Conclusions

A Pd–Mg/SiO_2 catalyst synthesized from a reverse microemulsion has been found to be active and selective for carbon dioxide methanation at 450 °C. The Pd–Mg/SiO_2 catalyst consists of Pd-containing aggregates within an amorphous Mg–Si oxide which are stable at reaction temperatures for 10 h and are significantly more active and selective than a similar catalyst synthesized first using a microemulsion to form Pd/SiO_2 followed by impregnation with Mg. In comparison to traditionally supported Pd/SiO_2 or Mg/SiO_2 catalysts the Pd–Mg/SiO_2 catalyst showed far higher selectivity for methane and greater CO_2 and H_2 conversion. Replacing the Mg with Fe or Ni maintained the high activity for carbon dioxide activation; however, the Fe-containing catalyst had little selectivity for methane. A bifunctional mechanism is proposed whereby the carbon dioxide is stabilized by the magnesium-containing oxide as a surface carbonate and sequentially hydrogenated to form methane. Ongoing work will precisely define the presence of the intermediates of the speculative mechanism to hopefully allow a better understanding and control of carbon dioxide utilization chemistry.

Acknowledgments

This work was supported by the US Department of Energy under Grant No. DE-FG02-89ER14048 and the experiments made use of the UCSB Materials Research Laboratory (MRL) Central Facilities supported by the MRSEC Program of the National Science Foundation under Award No. DMR05-20415 and the California Nanoscience Institute.

Appendix A. Supplementary data

Supplementary data associated with this article can be found, in the online version, at doi:10.1016/j.jcat.2009.05.018.

References

[1] S.E. Park, Y.S. Yoo, Stud. Surf. Sci. Catal. 153 (2004) 303–314.
[2] D.R. Burri, K.-M. Choi, J.-H. Lee, D.-S. Han, S.-E. Park, Catal. Commun. 8 (2007) 43–48.
[3] K.P. Brooks, J.L. Hu, H.Y. Zhu, R.J. Kee, Chem. Engin. Sci. 62 (2007) 1161–1170.
[4] G.M. Shashidhara, M. Ravindram, React. Kinet. & Catal. Lett. 37 (1988) 451–456.
[5] S. Furukawa, M. Okada, Y. Suzuki, Energy & Fuels 13 (1999) 1074–1081.
[6] M. Yamasaki, H. Habazaki, K. Asami, K. Izumiya, K. Hashimoto, Catal. Commun. 7 (2006) 24–28.
[7] H. Habazaki, M. Yamasaki, A. Kawashima, K. Hashimoto, Appl. Organometal. Chem. 14 (2000) 803–808.
[8] J.M. Rynkowski, T. Paryjczak, A. Lewicki, M.I. Szynkowska, T.P. Maniecki, W.K. Jozwiak, React. Kinet. & Catal. Lett. 71 (2000) 55–64.
[9] M. Marwood, F. Vanvyve, R. Doepper, A. Renken, Catal. Today (1994) 437–448.
[10] Z.-G. Zhang, G. Xu, Catal. Commun. 8 (2007) 1953–1956.
[11] S. Mori, W.C. Xu, T. Ishidzuki, N. Ogasawara, J. Imai, K. Kobayashi, Appl. Catal. A: Gen. 137 (1996) 255–268.
[12] M. Bowker, T.J. Cassidy, A.T. Ashcroft, A.K. Cheetham, J. Catal. 143 (1993) 308–313.
[13] T. Inui, M. Funabiki, Y. Takegami, React. Kinet. & Catal. Lett. 12 (1979) 287–290.
[14] C. de Leitenburg, A. Trovarelli, J. Kaspar, J. Catal. 166 (1997) 98–107.
[15] M. Tsuji, T. Kodama, T. Yoshida, Y. Kitayama, Y. Tamaura, J. Catal. 164 (1996) 315–321.
[16] J. Sehested, K. Larsen, A. Kustov, A. Frey, T. Johannessen, T. Bligaard, M. Andersson, J. Nørskov, C. Christensen, Topics Catal. 45 (2007) 9–13.
[17] Y.P. Hu, H.F. Jin, J.R. Liu, D.S. Hao, Chem. Engin. Journal 78 (2000) 147–152.
[18] A. Trovarelli, C. de Leitenburg, M. Boaro, G. Dolcetti, Catal. Today 50 (1999) 353–367.
[19] M. Boutonnet, S. Logdberg, E.E. Svensson, Curr. Opin. Colloid Interface Sci. 13 (2008) 270–286.
[20] S. Eriksson, U. Nylen, S. Rojas, M. Boutonnet, Appl. Catal. A & Gen. 265 (2004) 207–219.
[21] V. Uskokovic, M. Drofenik, Surf. Rev. & Lett. 12 (2005) 239–277.
[22] Y. He, B. Yang, G. Cheng, Catal. Today 98 (2004) 595–600.
[23] H. Li, J. Liu, S. Xie, M. Qiao, W. Dai, H. Li, J. Catal. 259 (2008) 104–110.
[24] T. Masui, K. Fujiwara, K.-i. Machida, G.-y. Adachi, T. Sakata, H. Mori, Chem. Mater. (1997) 2197–2204.
[25] A. Borodzinski, G.C. Bond, Catal. Rev. Sci. Eng. (2006) 91–144.
[26] P. Albers, J. Pietsch, S.F. Parker, J. Mol. Catal. A: Chem. 173 (2001) 275–286.
[27] Y. Schuurman, C. Mirodatos, P. Ferreira-Aparicio, I. Rodríguez-Ramos, A. Guerrero-Ruiz, Catal. Lett. 66 (2000) 33–37.
[28] J. Galuszka, Catal. Today (1994) 321–331.
[29] Y.G. Chen, K. Tomishige, K. Yokoyama, K. Fujimoto, Appl. Catal. A: Gen. 165 (1997) 335–347.
[30] J.N. Park, A.J. Forman, W. Tang, J.H. Cheng, Y.S. Hu, H.F. Lin, E.W. McFarland, Small 4 (2008) 1694–1697.
[31] S.J. Choe, H.J. Kang, S.-J. Kim, S.-B. Park, D.H. Park, D.S. Huh, Bull. Korean Chem. Soc. 26 (2005) 1682–1688.
[32] L.F. Liotta, G.A. Martin, G. Deganello, J. Catal. 164 (1996) 322–333.
[33] N. Yoshida, T. Hattori, E. Komai, T. Wada, Catal. Lett. 58 (1999) 119–122.